CHAPTER 10

THERMAL CONDUCTIVITY OF THE EARTH'S DEEPEST MANTLE

ANNE M. HOFMEISTER

Department of Earth and Planetary Sciences, Washington U., 1 Brookings Dr., St. Louis, MO 63130-4899, USA;
E-mail: hofmeist@wustl.edu

Abstract
Thermal transport properties in the lowest mantle are estimated, due to experimental limitations. The lattice component of thermal diffusivity (D) is constrained through measurements of dense phases made using the laser-flash technique, which is accurate ($\pm 2\%$) and unaffected by spurious radiative transfer. Thermal diffusivity is constant once a critical temperature (T_{sat}) of $\sim$1100 to 1500 K is exceeded. The saturated mean free path (λ_{sat}, computed from D_{sat} and sound velocities) nearly equals the primitive lattice parameter $<a>$. This relationship provides temperature independent values of D and k_{lat} for the lower mantle. Pressure derivatives are predicted by the damped harmonic oscillator model. An effective thermal conductivity, $k_{rad}(T)$, due to diffusion of heat by photons is estimated from optical spectra of perovskite at 298 K. To represent the internally heated, grainy mantle, our formulation accounts for grain-size (d) dependences of emissivity and physical scattering, and for interface reflections. An approximate analytical solution is derived which indicates that k_{rad} depends nearly linearly on T in the lower mantle. For perovskite (and probably post-perovskite), k_{rad} has a maximum at $X \sim 0.05$ Fe/(Mg + Fe) for $d \sim 1$ mm. At $X \sim 0.1$, k_{rad} is maximized at $d \sim 3$ mm. Our approximation overestimates k_{rad} at large X and d. For low spin Fe, k_{rad} is low due to grain-size effects, and reaches a maximum at high Fe content. Plumes are expected to form under destabilizing conditions of low thermal conductivity and negative $\partial k/\partial T$. The latter condition is unlikely in the deep mantle, but the following physical properties lower k_{rad}: large grains or very, very small grains, low Fe contents for low spin Fe, or high Fe contents for high spin Fe. High degrees of solid solution reduce k_{lat}. If localized Fe enrichment of the deepest mantle by core material occurs this could create plumes which would carry some core material upwards, thereby enriching the lower mantle in Fe with respect to the upper mantle, and leading to a gravitationally stable, chemically stratified mantle.

D. A. Yuen et al. (eds.), Superplumes, 269–292.
© 2007 *Springer.*

1 INTRODUCTION

Numerical convection models of the Earth have shown that the functional form for thermal conductivity (k) and its close relative thermal diffusivity:

$$D = \frac{k}{\rho C_P}, \tag{1}$$

where ρ is density and C_P is heat capacity at constant pressure (P), strongly influence the character of the solutions through feedback in the temperature equation. Accurately characterizing k or D as a function of T is thus essential to modeling planetary heat flow on diverse scales (e.g., Gerbault, 2000; Branlund et al., 2000; Yuen et al., 2000; Dubuffet et al., 2002; van den Berg et al., 2004; Yanagawa et al., 2005). The functional form of $k(T)$ is determined by summing the contributions from two different microscopic processes: (1) Transport of heat by scattering of phonons within each individual mineral grain is termed lattice conductivity ($k_{\rm lat}$): (2) Heat is also moved when photons emitted by any given grain in the medium are absorbed by nearby grains. Diffusive radiative processes are described by an effective thermal conductivity ($k_{\rm rad}$).

Many studies of $k(T)$ or $D(T)$ utilize contact methods such as that of Ångstrom. A significant problem is that silicates and oxides permit unwanted, direct radiative transfer above $\sim$500–800 K, as indicated by the reversal of the sign of $\partial k/\partial T$ from negative to positive near such temperatures (e.g., Kanamori et al., 1968; Lee and Kingery, 1960). However, the measurements are compromised at significantly lower temperatures because the radiative component increases gradually with temperature, and thus a small component exists at T below the reversal. Such boundary-to-boundary radiative transfer results when the material is transparent in some segment of the near-IR to visible spectrum. Most minerals behave in this manner. Contact methods do not permit differentiation of the two components, which is needed for geodynamic models, and they have systematic errors such those arising from thermal contact resistance, and are limited to $T < 1200$ K (e.g., Parker et al., 1961; Ross et al., 1984).

The present paper constrains the lattice component to $D(T)$ for deep mantle phases by applying the laser-flash technique (Parker et al., 1961) to structural analogues. The method is related to that of Schilling (1999), but accesses higher temperatures, avoids used of thermocouples, and removes remnants of boundary-to-boundary radiative transfer using the quantitative analysis of Mehling et al. (1998). We find D to be constant at mantle temperature and that this saturation value is related to the lattice parameter (Hofmeister, 2006), which is known or calculable.

Calculations of $k_{\rm rad}$ based on spectral data (e.g., Shankland et al., 1979) represent a *diffusive* process that fundamentally differs from boundary-to-boundary radiative transfer and thus cannot be extracted from laboratory measurements of k. Radiative transfer in the mantle is solely diffusive, as assumed in geodynamic models, as shown by estimating the effect of scattering in this grainy medium: If a tiny amount (0.005%) of light back-reflects from grain boundaries, then light is essentially extinguished over

distances of 2 to 200 m. Mantle gradients are below 10 K/km which makes it unlikely that light emitted from any given grain will reach another grain with temperature differing by 1 K. Physical scattering is important which means the grain size (d) cannot be ignored in calculations of k_{rad}. A recent model which includes the effect of d (Hofmeister, 2004a, 2005) is used to set limits on k_{rad} in the deepest mantle. Implications of the results for k_{lat} and k_{rad} on plumes arising from the deep mantle are briefly discussed.

2 LATTICE THERMAL CONDUCTIVITY

2.1 Theory

The quantum mechanical phenomena of phonon–phonon scattering transports heat through the lattice. Models of heat transport in insulators are based on Debye's (1914) analogy of the behavior of phonons to collisions of molecules in a gas, which provided:

$$k_{\text{lat}} = \frac{\rho}{3ZM} C_V u^2 \tau, \tag{2}$$

where ρ is the density, M is the molar formula weight, Z is the number of formula units in the primitive unit cell, τ is the mean free lifetime, and u is an acoustic velocity. The factor ρ/ZM accounts for typical units of heat capacity (per mole of formula unit).

As is the case for heat capacity, models for k_{lat} used either parameters for acoustic modes or parameters for optic modes. Historically, the problem in modeling k_{lat} lies in determining the lifetime, or equivalently the mean free path (λ), of phonon–phonon collisions (Ziman, 1962). Lifetimes in acoustic models are roughly estimated (Roufosse and Klemens, 1973), whereas lifetimes in optic models are extracted from quantitative IR spectra using the damped harmonic oscillator model of Lorentz (Hofmeister, 1999, 2001). The next subsections summarize the form for $k_{\text{lat}}(T)$ predicted by both types of models, and use these to determine the temperature dependence of D.

2.1.1 Acoustic models for the temperature dependence of thermal conductivity

Because heat capacity is a complicated function of T, low- and high-temperature limits have been the focus of acoustic models. The high-T limit is considered here.

For T greater than the Debye temperature (θ), Peierls (1929, 1956) assumed that the mean free path goes $1/T$ which leads to

$$k_{\text{lat}} = B/T \quad \text{for} \quad T > \theta. \tag{3}$$

Dugdale and MacDonald (1955) obtained Equation 3 using dimensional analysis. Their proportionality constant differs from those of Julian (1965) and Roufosse and Klemens (1973) whose values of B differ by a factor of $\sim$7. Because heat capacity is nearly constant for $T > \theta$, Equation 3 gives the limit $D \propto 1/T$.

Equation 3 is invalid if temperature is high enough that the mean free path becomes shorter than the unit cell (e.g., Ziman, 1962). Roufosse and Klemens (1974) obtained

the relationship:

$$k_{\rm lat} = \frac{B}{T}\left[\frac{2}{3}\left(\frac{C}{T}\right)^{1/2} + \frac{1}{3}\frac{T}{C}\right] \quad \text{for } T > \theta, \tag{4}$$

where the constant C is related to the Debye frequency and is proportional to $N^{2/3}$. For simple solids, $N \sim 1$ or 2, C is $\sim$500 K, and deviations from Equation 3 of $\sim$15% are seen only above twice this temperature. For complex crystal structures with $N \sim 10$, C should be 1000–2000 K. Thus Equation 3, rather than Equation 4, should be valid up to the melting temperatures of minerals (Roufosse and Klemens, 1974). Liebfried and Schlöman (1954) independently reached this conclusion.

The above results were obtained by assuming three phonon collisions. For four-phonon events and $T > \theta$, Pomeranchuk (1943) found that $k_{\rm lat} \sim T^{-5/4}$. Klemens (1969) and Ziman (1962) respectively suggested the forms:

$$k_{\rm lat} \sim \frac{1}{BT + CT^2}, \quad \text{or} \quad k_{\rm lat} \sim \frac{1}{BT} + \frac{1}{CT^2}. \tag{5a,b}$$

Because $T > \theta$, the same approximate forms could be used to describe D.

2.1.2 The damped harmonic oscillator model of thermal diffusivity

The optic model is developed in Hofmeister (1999, 2001, 2004b), Geisting and Hofmeister (2002), and Geisting et al. (2004). The lifetime of any given optic mode, τ_i, equals $1/2\pi\,\mathrm{FWHM_i}$, where FWHM is the full width at half maximum of peaks in the dielectric functions obtained from IR reflectivity data (e.g., Spitzer et al., 1962). The FWHM for each mode describes its interaction with all other vibrational modes in real crystals, including acoustic, and includes the effects of mode mixing, anharmonicity, disorder, impurities, and defects. FWHM can also be obtained from Raman spectra.

Due to a lack of information regarding the specific dependence of frequency on wavevector for each mode, average properties are used:

$$k_{\rm lat} = \frac{\rho}{3ZM}\frac{C_V <u>^2}{2\pi <\mathrm{FWHM}>}. \tag{6}$$

Because velocities of acoustic and optic modes should be similar inside the Brillouin zone, as inferred from theoretical and measured dispersion relations, acoustic velocities are averaged to provide $<u>$. A simple average of the compression and shear speeds is used here. Other averages are possible, and the specific form for $<u>$ depends somewhat on the crystal structure (Hofmeister, 2004c).

Combining Equations 1 and 6, and neglecting the ($\sim$1–3%) difference between C_P and C_V, provides the temperature dependence of the thermal diffusivity:

$$D(T) = \frac{<u(T)>^2}{6\pi Z <\mathrm{FWHM}(T)>} = \frac{u(T)\lambda(T)}{3Z}. \tag{7}$$

The factor of M is cancelled because Equation 1 presumes C_P has units J/g-K.

The temperature dependence of D (Eq. 7) is inferred as follows: Sound velocities of dense minerals depend weakly on temperature: $\partial(\ln u)/\partial T$ is near -0.004%/K for dense phases such as garnets (Anderson and Isaak, 1995). Derivatives for dielectric peak widths are ~ 100 times larger, $\partial(\ln \mathrm{FWHM})/\partial T = 0.25\%$/K near 298 K for MgO (Kachare et al., 1972) and thus the temperature dependence of D is derived from the response of FWHM. This information, Equation 7, and observation of finite peak width for MgO at 4 K (Kachare et al., 1972) lead to the following form:

$$\frac{1}{D} = \frac{6\pi Z}{u_0^2}(\mathrm{FWHM}_0 + aT)(1 + bT + cT^2) \approx A + BT + CT^2 + \cdots, \qquad (8)$$

where a, A, etc. are constants (Hofmeister, 2006). The coefficient B dominates and has a positive sign. This form best fit measurements of garnets, which reached the saturation limit (Hofmeister, 2006). If T_{sat} is not reached or $\partial(\ln u)/\partial T$ is not weak, then forms such as $D = a + b/T + c/T^2 + dT^3$ represent the data well (Pertermann and Hofmeister, 2006).

Pressure does not alter the population of the vibrational levels or the other factors thought to influence FWHM. Using Equation 7, and assuming that the mode Grüneisen parameters on average equal the thermal Grüneisen parameter gives

$$\frac{\partial(\ln(D))}{\partial P} = \frac{2}{K_T}\left(\gamma_{\mathrm{th}} + \frac{1}{3}\right). \qquad (9)$$

2.2 Experiment

The fast, contact-free method of Parker et al. (1961) was used to determine thermal diffusivity, wherein a sample in the form of a small slab with parallel faces is held at temperature in a furnace while emissions from the top of the slab are monitored remotely with an IR detector. We use plates with parallel surfaces of thickness of 0.6–2.0 mm and diameters of 8–15 mm with sand-blasted surfaces. The bottom of the slab is heated above the furnace temperature by an optical pulse from an IR laser. Top and bottom surfaces of the sample are graphite coated to enhance absorption of the laser pulse, to shield the detector from laser light, and to increase the intensity of sample emissions (Blumm et al., 1997). Usually, samples are sputter coated with Au or Pt metal before application of graphite to maximize suppression of boundary-to-boundary radiative transfer. As heat from the laser pulse diffuses from the bottom to the top of the sample, the increase in emissions is recorded by the IR detector, in the form of a temperature–time curve. Because boundary-to-boundary transfer is difficult to eliminate at high temperature, its effect on temperature–time curves is incorporated in data analysis (Tan et al., 1991; Andre and Degiovanni, 1995; Mehling et al., 1998; Hofmann et al., 1997). The temperature dependence of D is determined by varying furnace temperature. The pulse must be shorter than the time it takes heat to cross the sample, which is easily achieved with a laser. Because the change in temperature associated with the pulse is small, $\sim$4 K, D is approximately constant during the measurements, simplifying analysis (Parker et al., 1961).

We use a Netzsch LFA 427 apparatus which covers temperatures from ~290 to 2200 K under an Ar atmosphere. Main components are an evacuable furnace with a graphite heating element, water cooled housing, a Nd-GGG laser, and an InSb detector. For a detailed description, see Braeuer et al. (1992) and Blumm and Lemarchand (2002).

Temperatures were monitored using a type D W/Re thermocouple, which was calibrated against Curie transition points of metals. Thermal diffusivity values were calibrated against electrolytic iron, austenitic stainless steel, and Poco graphite standards (Hendersen et al., 1998). Data were collected at intervals of 50 to 100 K as each sample was heated to some maximum temperature. If the sample was not melted, data were also collected during the cool down. Three measurements were made at each temperature step.

2.3 Results

For all minerals studied so far using the laser-flash apparatus, thermal diffusivity decreases rapidly as temperature increases above ambient temperature, such that the slope $\partial D/\partial T$ gradually decreases as T increases until D asymptotically approaches a constant at high temperature (Hofmeister, 2004b, 2006; Pertermann and Hofmeister, 2006). Figure 1 provides examples. The shape of the curve for $D(T)$ depends on chemical composition and structure, but constant D exists at some high temperature for all crystalline substances, except for a few cases where melting occurred while D

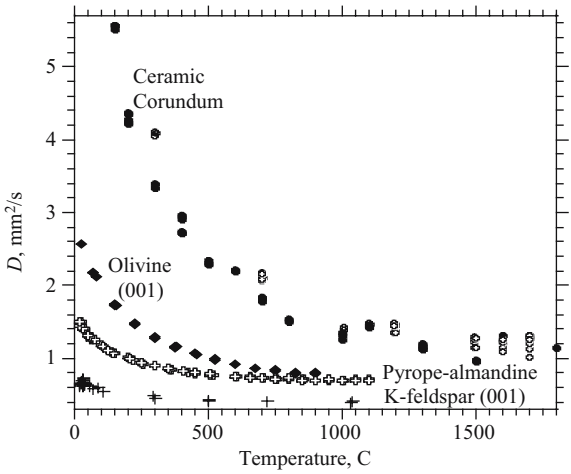


Figure 1. Thermal diffusivity as a function of temperature for minerals with various structures. Filled and open circles = two different samples of ceramic corundum Al_2O_3 with low porosity. Diamond = olivine, $Mg_{0.9}Fe_{0.1}SiO_4$, the (001) face. Plus = feldspar, $KAlSi_3O_8$, the (001) face. Open cross = randomly oriented garnet, $(Mg_{0.43}Al_{0.53}Ca_{0.04})_3Al_2Si_3O_{12}$. Data from Pertermann and Hofmeister (2006) and Hofmeister (2006).

was still decreasing (e.g., calcic garnets). The temperature of saturation is higher for end-member compositions (e.g., Al_2O_3, MgO), than for solid solutions (e.g., most natural garnets) or disordered minerals (e.g., feldspar, Fig. 1).

2.3.1 Comparison of the temperature dependence of D with theory

The observed non-linear decrease in D with temperature (Fig. 1) is not consistent with acoustic models (Eqs. 3–5), although addition of a constant to Equation 5a would provide a form for $D(T)$ that is compatible with our results up to T_{sat}. Acoustic models do not predict a high temperature asymptote for minerals due to their high Debye temperatures (Roufosse and Klemens, 1974).

The dependence of D on temperature is consistent with the damped harmonic oscillator model (Eq. 8). Our measurements (Fig. 1) show that the FWHM controls the temperature dependence of D insofar as u depends weakly on temperature for most dense minerals (Anderson and Isaak, 1995).

Achievement of constant D at high T is also consistent with the damped harmonic oscillator model. In the kinetic theory of gases, lifetimes are connected with the number of molecules per unit volume (e.g., Reif, 1965). At 298 K, FWHM of diverse crystalline structures roughly depends on the number of phonons within the primitive unit cell (Hofmeister, 2004c). As temperature increases, overtone-combination modes are excited. Saturation in the number of modes occurs when T is sufficiently high that the phonon continuum dominates the statistics (Mitra, 1969), and increasing T no longer changes the number of phonons, but rather increases their energy. The flat trend in D at high T occurs when $k_B T \sim h\nu$ of the overtones, where k_B is Boltzmann's constant and h is Planck's constant, which is consistent with phonon saturation. As ρ weakly decreases at high T and C_P weakly increases, k_{lat} (Eq. 1) is also independent of T at roughly double the Debye temperature (Hofmeister and Yuen, under review).

Asymptotic flattening of D is analogous to the Dulong-Petit limit of 3R (the gas constant) for C_P at high T (Fig. 1) and constitutes a threshold (Hofmeister and Yuen, under review). Another threshold temperature divides the strongly T-dependent regime at moderate temperatures ($\sim$250 to $\sim$1200 K) from the cryogenic regime where $1/D \sim T^n$ such that $n \sim 2$–3 (Hofmeister, 2006). An analogy of $1/D$ exists with heat capacity, which is dominated by the behavior of acoustic modes at low T, optic modes at high temperature, and saturation at very high temperature. The regimes for $C_P(T)$ result from populations of energy levels changing with temperature. Phonon–phonon interactions, described by FWHM, should also increase as more energy levels are populated. Thus, $1/D$, being proportional to FWHM, has a T-dependence like that of C_P.

2.3.2 Connection of the saturated mean free phonon path with lattice parameters

The mean free path of the phonons (Fig. 2) was obtained using Equation 7, results for $D(T)$ in Figure 1 and in Hofmeister (2006), and weighted average of the sound speeds

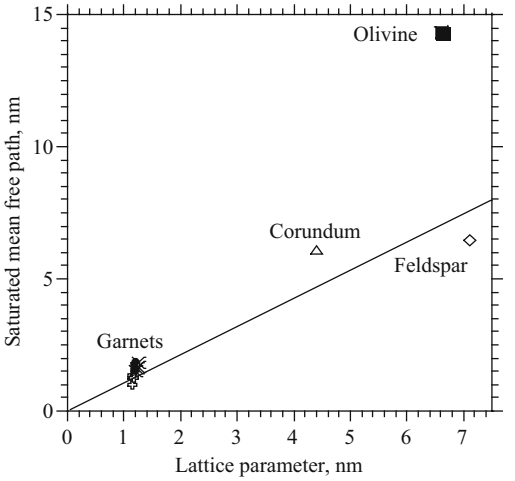


Figure 2. Relationship of the mean free path at saturation (Eq. 7) with lattice parameter for the substances in Figure 1, as labeled, garnet data from Hofmeister (2006). Cross = Mg-Fe-Al garnets; dot = calcic garnets; X = synthetics. Lattice parameters and acoustic velocities $<u> = (u_P + 3u_S)/3$ from the literature (e.g., Smyth and McCormick, 1995; Bass, 1995). Solid line = 1:1 correspondence.

for samples with a large number of vibrational modes (garnet, feldspar), a simple average for a moderate number (olivine) and $<u> = u_P$ for few vibrational modes (corundum), see Hofmeister (2004c). Because acoustic velocities depend linearly and weakly on temperature, $\lambda(T)$ follows $D(T)$. The mean free path is thus constant at high temperature, and approaches the lattice parameter (Fig. 2), which has been considered to a lower limit for λ (Ziman, 1962). It is not clear why olivine departs from the linear trend defined by all other samples. A wider range of mineral structures and chemical compositions needs to be examined to better constrain the dependence of λ on a.

2.3.3 Inference of deep mantle values of lattice thermal conductivity and diffusivity

For mantle materials, high temperatures are expected so constant D (and k_{lat}) will occur throughout the mantle. To determine D_{sat}, we therefore estimate λ_{sat} from Equation 7, using the primitive lattice constants $<a>$ of the phases expected to dominate the lowest mantle. The primitive unit cell, rather than the crystallographic, pertains because the type and number of phonons in a crystalline solid are represented by the vibrations of the primitive unit cell. From Figure 2, this approach approximates D and thus k_{lat}. There is quite a bit of uncertainty involved as olivine does not follow the 1:1 correspondence; although extensive solid solutions closely follow ($\lambda_{sat} = <a>$).

Table 1. Physical properties of $MgSiO_3$

Properties at 120 GPa, 0 K	Perovksite	Post-perovskite	Reference
Space Group	*Pbnm*	*Cmcm*	
Z (primitive)	4	2	
Volume, Å^3 (crystallographic)	122	120	Iitaka et al. (2004)
$<a>$, Å (primitive)	4.96	3.92	Calculated from V
u_P, km/s	~13.5	~14	Iitaka et al. (2004)
u_S, km/s	~7.5	~7.5	Iitaka et al. (2004)
D_{sat}, mm^2/s	3.92	6.33	This work
$k_{lat,sat}$, W/m-K	5.37	8.7	This work
K_T, GPa	660	654	Iitaka et al. (2004)
Properties at ambient conditions			
K_T, GPa	248	222	Tsuchiya et al. (2004)
dK/dP	3.9	4.2	Tsuchiya et al. (2004)
γ_{th}	1.55	1.64	Tsuchiya et al. (2004)

The relevant physical properties (Table 1) are based on calculations, some of which are confirmed experimentally. Measurements of Organov and Ito (2004) at 118 GPa and 300 K provide a volume for post-perovskite (ppv) that is 1% higher, whereas results of Murakami et al. (2004) are essentially the same as the calculations. Thermal conductivity is determined from Equation 1, using density from PREM $= 5.5$ g/cm^3 (Dziewonski and Anderson, 1981) and $C_P \sim 3\mathrm{R} = 24.9$ J/mol, and 101 g/mol for both ppv and perovskite (pv) magnesium end-members.

From Equation 9 and Table 1, the pressure dependence of D is $\sim 0.6\%$/GPa near 120 GPa, and thus is negligible in the core-mantle boundary region. Near 22 GPa, $\partial(\ln(D))/\partial P$ is $\sim 1.2\%$/GPa. Approximating λ as $<a>$ creates more uncertainty than neglecting the effect of pressure over the lower mantle. Thus, the estimates at 120 GPa (Table 1) represent the lower mantle. Notably, ppv is much more effective at transporting heat than pv. As the difference is largely due to disparate sizes of the primitive unit cells, other compositions of these mantle phases, e.g., $(Mg_{0.9}Fe_{0.1})SiO_3$ (Mao et al., 2004), will have similar relative values.

3 RADIATIVE THERMAL CONDUCTIVITY

Realistically modelling the hot lower mantle requires quantifying any heat moved diffusively by photons. This process is described by an effective thermal conductivity (k_{rad}) that cannot be extracted from laboratory measurements because a different type of radiative transfer occurs therein, termed boundary-to-boundary. In the latter process, light from the source warms the thermocouple with negligible participation of the sample (e.g., Kanamori et al., 1968; Lee and Kingery, 1960). By constrast, diffusion of photons occurs by sequential emission and absorption of light from grain-to-grain,

and k_{rad} is calculated from optical spectra. A new formulation (Hofmeister 2004a; 2005) accounts for the frequency dependence of emissivity, in accord with radiative transfer models depicting diverse situations (e.g., Brewster, 1992; Evans, 1992; Kaufmann and Freedman, 2002; Hapke, 1993). The model accounts for the two effects of grain-size (d): physical scattering which shortens the photon's mean free path (Fujisawa et al., 1968), and reflection at interfaces which reduces throughput, especially at frequencies where absorbance is high. As a result, k_{rad} depends strongly and non-linearly on grain-size.

Spectra are currently unavailable for ppv, and available spectra of pv are inadequate for the calculation, having baseline problems due to scattering. Therefore, this paper uses the general behavior of $k_{rad}(T)$ at high temperature to describe the lower mantle.

3.1 Spectra of mantle minerals

Figure 3 shows the three types of optical spectra observed so far for mantle minerals. For details of the technique, see Rossman (1988) and other papers cited in this section.

Olivine has Fe^{2+} in 6-coordination. Octahedral sites have similar sizes in various minerals, and patterns like that of olivine (Fig. 3) were observed for orthopyroxene, clinopyroxene, wadsleyite, silicate spinels, and magnesiowüstite (Burns, 1970; Goto et al., 1980; Rossman, 1988b; Ross, 1997; Smith and Langer, 1982).

Polycrystalline majorite has three weak peaks at low frequency, assigned to Fe^{2+} in the large 8-coordinated site, as in low-pressure garnets (Fig. 3). The high frequency,

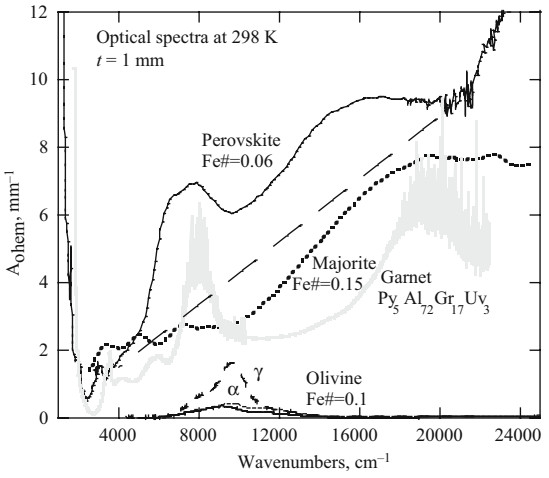


Figure 3. Near-IR to visible spectra of mantle silicates. Light lines = three polarizations of gemmy olivine as marked (Taran and Langer, 2001). Grey = garnet (this work); Heavy dots = majorite (Keppler and McCammon, 1996). Solid line = perovskite (Keppler et al., 1994). Long dashed line = rough baseline for scattering. Iron contents as indicated. Intensities of the high pressure phases are approximate due to uncertainties in both thickness and in the baseline correction.

broad peak was attributed to Fe^{2+}-Fe^{3+} charge transfer (Keppler and McCammon, 1996); but charge transfer bands in low-pressure garnets are narrower (Fig. 3) and seen at high Fe contents (Khomenko et al., 2002). The absorbance of the high ν peak is uncertain as the baseline is equivocal. Due to these problems, $k_{\rm rad}$ of majorite is not computed here.

Polycrystalline perovskite has two d-d electronic transitions of Fe^{2+} from ~6500–8000 cm^{-1} superimposed on a strong scattering curve (Fig. 3) for its 8-coordinated site. A third high frequency band was assigned to charge transfer (Keppler et al., 1994). If Fe ions are is randomly distributed among the octahedral and 12-coordinated sites, then 5% of the Fe^{2+} atoms have Fe^{3+} as neighbors. Probably the juxtaposition is lower: local compensation of charge suggests that octahedral Fe^{3+} should instead be balanced by Fe^{3+} in an adjacent dodecahedra, which is consistent with an uncertain site occupancy of Fe^{3+}(McCammon et al., 1992). Given that the intensity of the ~16, 000 cm^{-1} band is similar to those of the low frequency Fe^{2+} transitions, this peak may also be a d-d transition, since three are expected from symmetry. Alternatively, Fe^{3+} is interstitial, e.g., magnetite particles, or on grain boundaries, producing a high frequency band which is not intrinsic to perovskite. Mie scattering from particles does produce peaks at such frequencies (Khomenko et al., 2002). In lieu of single-crystal spectra, radiative transfer for perovskite is calculated with and without the highest frequency band.

Visible spectra have not been measured for post-perovskite, but the cation sites where Fe resides in these two phases are similar (Murakami et al., 2004; Tsuchiya et al., 2004; Mao et al., 2004), suggesting that their absorption spectra will be similar enough that radiative transfer in the lower is not affected by this phase transition.

Visible spectra do not exist for low spin states of any silicate, but it is expected that the pattern consists of very weak bands in the visible and a UV tail.

3.2 Theory

For local radiative equilibrium, optically thick conditions, and non-opaque media:

$$k_{\rm rad}(T) = \frac{4\pi}{3}\int_0^\infty \left(\frac{d}{1+dA(\nu,T)}\right)\frac{c}{\nu^2}\frac{\partial}{\partial T}\left\{[n(\nu,T)]^2[1-{\rm e}^{-dA(\nu,T)}]I_{\rm bb}(\nu,T)\right\}d\nu. \tag{10}$$

where $[d/(1+dA)]$ is the mean free path, n is the index of refraction, c is the speed of light, ν is frequency in cm^{-1}, T is temperature, and $I_{\rm bb}$ is Planck's blackbody function with energy-density provided on a per wavelength basis (Hofmeister, 2004a, 2005). Attenuation of light is described by the true absorption coefficient:

$$A = -\frac{1}{d}\ln\left(\frac{I_{\rm tra}}{I_0}\right), \tag{11}$$

where $I_{\rm tra}$ is the transmitted intensity, I_0 is the incident intensity, and d is thickness or grain-size (Brewster, 1992). The conventions in geophysical literature re followed

except that $\nu = 1/\lambda$, as used in mineral spectroscopy. The factor $[1 - e^{-dA}] = \xi$, the emissivity, was defined by Kirchhoff in ca. 1865. An average grain-size and absorption coefficient are used to describe the mantle, which parallels representation of viscous damping in geodynamic models (Ranalli, 2001).

In evaluating Equation 10, an additional physical process in a grainy medium must be accounted for. Namely, that the amount light exitting the grain is reduced from the incident intensity not only by losses from absorption (Eq. 11), but also due to back reflections (R) at the surface (Hofmeister, 2004a, 2005). This step is necessary because back reflections and high absorbance together produce opaque spectral regions and the model is not valid when the grains are opaque (Clark, 1957). Thus, frequency regions where no light is transmitted must be excluded when integrating Equation 10. How back reflections reduce throughput (and thus radiative transfer) in mantle grains is understood by comparison to laboratory measurements. Absorbance ($a_{\rm chem}$) is obtained from measurements of transmission which include not only $I_{\rm tra}$ (Eq. 11) but also a reduction in throughput due to reflection. Because common logarithms are often used:

$$Ad = 2.3026[a_{\rm chem} + 2\log(1 - R)], \tag{12}$$

where R is computed from the index of refraction mismatch at grain interfaces using Snell's law and Fresnel's equations. Opacity occurs when the product $dA(\nu)$ reaches a critical value, controlled by R, such that the light from any given grain cannot reach its second-nearest neighbor. Such sections are excluded from the integral. This chapter considers the case $dA < 7$ ($R \sim 0.1\%$), corresponding to subhedral grain with $\sim$120° angles, common in mantle rocks. Other cases (Hofmeister, 2005) give similar results.

Given that radiative transfer models are approximate, Equation 10 is simplified based on the dependence of material properties on ν, T, and P. The near-IR to UV spectral range need only be considered, as the lattice modes in the far- to mid-IR, and the metal-oxygen charge transfer bands in the far-UV are too intense to permit radiative transfer. The result (Hofmeister, 2005) is:

$$k_{\rm rad}(T) = \frac{4\pi\, dn^2}{3} \sum \int_{lower}^{upper} \frac{(1 - e^{-dA})}{(1 + dA)\nu^2} \frac{\partial[I_{\rm bb}(\nu, T)]}{\partial T} d\nu, \tag{13}$$

where the sum allows for transparent regions existing above and below the strong bands in the visible. Because A is a complex function of ν (next section) and the cutoff frequencies depending on d and A, Equation 13 is evaluated numerically.

3.2.1 Why the effect of pressure can be neglected

The pressure dependence of the material properties determines $k_{\rm rad}(P)$. Values of $\partial n/\partial P$ are sufficiently small that this aspect can be neglected. The relevant quantity is then $(\partial A/\partial\nu)(\partial\nu/\partial P)$. Although peaks shift with pressure, values of $\partial\nu/\partial P$ at 298 K are near or equal to zero for many bands (Burns, 1982). Moreover, $\partial A/\partial\nu$ is positive at frequencies below the central frequency, but negative above. Combining these effects provides very small values of $\partial k_{\rm rad}/\partial P$, especially when the peak is contained

entirely within the blackbody curve (above ~ 1900 K for Fe^{2+} absorptions of mantle minerals). Thus, $\partial k_{\rm rad}/\partial P$ is unimportant. See Hofmeister (2005) for details.

Furthermore, from the Beer-Lambert law, A is proportional to the concentration. Since concentration is unaffected by pressure, neither should $k_{\rm rad}$ change with pressure.

3.2.2 Use of asymptotic limits to estimate $k_{\rm rad}$

For nearly transparent materials:

$$k_{\rm rad}(T) \cong \frac{4\pi d^2 n^2}{3} \sum \int_{lower}^{upper} \frac{A}{\nu^2} \frac{\partial [I_{\rm bb}(\nu, T)]}{\partial T} d\nu, \quad \text{for } dA \text{ small.} \tag{14}$$

Thus, as $A \to 0$, $k_{\rm rad} \to 0$. Diffusive radiative transfer is absent in a fully transparent medium because a photon cannot heat a grain unless it is absorbed. As $d \to 0$, $k_{\rm rad} \to 0$. This case approximates exceedingly fine-grained ceramics that are effectively opaque due to back reflections. Physical scattering dominates this asymptotic limit.

For dark materials, Equation 13 reduces to the result of Shankland et al. (1979):

$$k_{\rm rad}(T) \cong \frac{4\pi n^2}{3} \sum \int_{lower}^{upper} \frac{1}{A\nu^2} \frac{\partial [I_{\rm bb}(\nu, T)] \partial T}{\partial T} d\nu, \quad \text{for } dA \text{ large.} \tag{15}$$

For an opaque medium ($A \to \infty$) and for any value of d, the correct limit ($k_{\rm rad,dif} \to 0$) is obtained. When dA exceeds a critical value depending on reflectivity and texture (discussed above), $k_{\rm rad,dif} \to 0$. The result of Shankland et al. (1979), derived without considering grain-size, is invalid for very weakly absorbing regions unless grain-size is very, very large.

If A is independent of ν and T, then Equation 14, integrated from $\nu = 0$ to ∞, provides the following simple formula:

$$k_{\rm rad} = \frac{16}{3} \sigma T^3 d^2 A, \quad \text{for } dA \text{ small and constant,} \tag{16}$$

where σ is the Stefan-Boltzmann constant. For constant A, Equation 15 becomes

$$k_{\rm rad} = \frac{16}{3} \sigma T^3 \frac{1}{A}, \quad \text{for } dA \text{ large and constant.} \tag{17}$$

Equation 17 is Clark's (1957) result, which was derived without considering grain-size.

The form for $k_{\rm rad}(A)$ at intermediate values of dA is inferred by combining Equations 16 and 17. Because $\partial k_{\rm rad}/\partial A$ is positive at low dA but negative at high dA, and both limits for $k_{\rm rad}$ are 0, a maximum exists in $k_{\rm rad}(A)$: $k_{\rm rad}$ is largest for moderate A and moderate grain-size, where physical scattering is not overwhelming, significant light is emitted by individual grains in the mantle, and this light is not completely extiguished by neighboring grains. Because A is roughly proportional to

concentration, $k_{\rm rad}$ has a maximum in concentration as well, discussed by Hofmeister and Yuen (under review).

Radiative transfer is more complex than T^3 law in Equations 16 and 17 because A depends on n and T. However, the temperature dependence of $k_{\rm rad}$ can be inferred from these equations (Hofmeister, 2005; Hofmeister and Yuen, under review). The dependence of A on ν weakens the temperature dependence of $k_{\rm rad}$ as it truncates the integral of Equation 13. For small dA, A increasing with T strengthens the temperature dependence of $k_{\rm rad}$ (Eq. 16). The effects of $A(\nu)$ and $A(T)$ roughly cancel at small dA, suggesting for small dA, the T^3 law is roughly correct. But for large dA, A increasing with T decreases $k_{\rm rad}$ (Eq. 17). Dark samples are opaque over larger portions of the integral, which further decreases $k_{\rm rad}$. A much weaker dependence than T^3 is expected for $k_{\rm rad}$ at high T.

3.2.3 An approximate formula that connects $k_{\rm rad}$ with concentration

If the peak is narrow and Ad is low enough that the material is not opaque, then Equation 13 can be evaluated using the trapezoidal rule, providing:

$$k_{\rm rad}(T) = \frac{4dn^2}{3}\frac{[1-\exp(-dA_{\rm ave})]}{(1+dA_{\rm ave})}\Delta\nu\frac{2\pi {\rm h}^2{\rm c}^3\nu_{\rm ave}^4}{k_{\rm B}T^2}\frac{\exp({\rm hc}\nu_{\rm ave}/k_{\rm B}T)}{[\exp({\rm hc}\nu_{\rm ave}/k_{\rm B}T)-1]^2}, \quad (18)$$

where $\nu_{\rm ave}$ and $A_{\rm ave}$ represent the average frequency and average absorption coefficient for a peak that spans the interval $\Delta\nu$ (Hofmeister, 2004b). For a single band, $A_{\rm ave}$ equals the half height $= A_{\rm max}/2$. For broad or multiple peaks, $k_{\rm rad}$ could be calculated by summing the results for a series of segments, for example, $1/10^{\rm th}$ of each peak in the spectrum could be evaulated individually using Equation 18, as well as the near-IR and UV tails. As a first approximation, this paper considers a single peak by generalizing the derivation of Hofmeister (2004b) to cover species other than hydroxyl.

The Beer-Lambert law, which is valid for low to moderate concentrations:

$$X = \sum {\rm II}/(df''), \quad (19)$$

where $\sum$II is the sum of the integrated intensities for the three orthogonal directions, d is thickness or grain size, f, f' or f'' are extinction coefficients, is obtained by calibration (e.g., Rossman 1988b). A simplified version of the Beer-Lambert law is used here:

$$X = A_{\rm max}/f' = A_{\rm ave}/f. \quad (20)$$

The connection of X with A means that the temperature dependence of the spectra can be neglected in this approximation.

The variables in Equation 18 are separable. Combining Equations 18 and 20 gives

$$k_{\rm rad} = \vartheta(T)\frac{8\pi c k_{\rm B} dn^2}{3}\nu_{\rm ave}^2\Delta\nu\frac{1-\exp(-dfX)}{1+dfX}, \quad (21)$$

where the temperature function (ϑ) is given by

$$\vartheta(T) = \left(\frac{s}{T}\right)^2 \frac{\exp(s/T)}{[\exp(s/T) - 1]^2}, \tag{22}$$

and $s = \mathrm{hc}\nu_{\mathrm{ave}}/k_{\mathrm{B}}$. Materials with absorption bands do not follow the T^3 law of Clark (1957). The next section calculates $\vartheta(T)$ for mantle conditions.

Zeros exist in the derivative of Equation 21 taken with respect to concentration:

$$\frac{\partial[\ln(k_{\mathrm{rad}})]}{\partial X} = \frac{df}{[\exp(dfX) - 1]} - \frac{df}{(1 + dfX)}. \tag{23}$$

Equation 23 combined with k_{rad} being positive requires that maxima occur in k_{rad} with X. Given the form of Equations 21 and 23, maxima could also occur in k_{rad} with d. This analysis agrees with the asymptotic behavior of k_{rad} (Section 3.2.2).

To summarize, k_{rad} depends largely on how dark (i.e., Fe-rich) or how pale (i.e., very Fe-poor) individual grains are, more than on the specific spectrum possessed by a given mineral phase. Because completely opaque minerals do not transfer radiation, very Fe-rich minerals have low k_{rad}. Very Fe-poor minerals have low k_{rad} because these are poor emitters, and thus k_{rad} has a maximum at moderate [Fe^{2+}].

3.3 Results

3.3.1 Temperature behavior of k_{rad}

Figure 4 shows that ϑ monotonically increases with T for relevant band positions. The function climbs rapidly near $\sim$ 1500 K for the bands clearly due to d-d transitions of Fe^{2+}, is roughly linear over mantle temperatures, and flattens as T becomes very high. The dependence of s on ν_{ave} means that over mantle temperatures, the d-d transitions in perovskite provide $\vartheta(T)$ that is larger by a factor of 10 over $\vartheta(T)$ for the high frequency band (Fig. 3). Post-perovskite should behave the same.

Figure 4 shows that the temperature component of k_{rad} does not follow the T^3 law for materials with absorption bands. Over the temperature range shown, $\vartheta(T)$ can be fit to a second or third order polynomial, depending on the value of s. Similar behavior was seen for k_{rad} computed for olivine at small d using Equation 13 (Hofmeister, 2005). This correspondence is expected as Equation 22 was derived by assuming that dA is not so large that opacity occurs near ν_{ave}.

3.3.2 Grain size and Fe content dependence of k_{rad}

Calculation of k_{rad} from Equation 21 using the parameters in Table 2 provides approximate values because (1) Fe^{2+} bands are broad, not narrow and (2) surface reflectivity, which can cause opacity for high absorbance, is not accounted for. Large peak breadth contributes some errors, but the amount should be independent of d or X. For low values of absorbance $= dA \propto dX$, the results should be accurate, since opacity is unlikely. For some large value of dA (i.e., of dX), light is not transmitted at frequencies near the center of the peak and this frequency interval should not have been

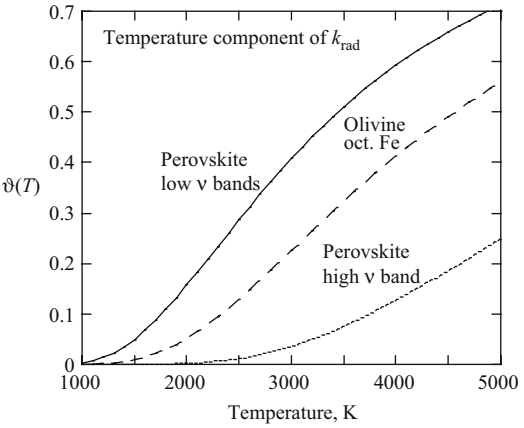


Figure 4. Dependence of ϑ (Eq. 22) on temperature. Three values of s are as follows: $\nu_{ave} = 7138$ cm^{-1} for the d-d transitions of Fe^{2+} in perovskite give $s = 21,870$ K; $\nu_{ave} = 9444$ cm^{-1} for octahedrally coordinated Fe^{2+} [olivine which proxies for (Mg,Fe)O] gives $s = 13,589$ K; and $\nu_{ave} = 15,200$ cm^{-1} for the third band in perovskite gives $s = 21,870$ K. At lower mantle temperatures ($\sim$2000–3000 K), the contribution to k_{rad} from high frequency bands is small, <10%.

Table 2. Spectral properties

	Pv low ν	Olivine	Pv high ν
X, mole%	0.06	0.10	0.06
A_{max}, cm^{-1}	35	8	24
ν_{ave}, cm^{-1}	7138	9444	15,200
$\Delta\nu$, cm^{-1}	3000	2500	6000
n	1.73	1.65	1.73
f, cm^{-1}	290	40	200

included in the integral. As dX increases, the frequency interval becomes larger. Thus, for larger and larger dX, k_{rad} is overestimated. This behavior will affect the trends with d and X.

If the high ν band of perovskite is intrinsic, then the corresponding $\vartheta(T)$ is 1/10th the value calculated for the low ν bands. The remaining components of k_{rad} (cf. Eqs. 21 and 22) depend on ν_{ave}, $\Delta\nu$, d and X. Because the strengths of the d-d transitions and the charge transfer bands in perovskite with high spin Fe^{2+} are essentially the same, the results in Figure 5, lower panels, need only be scaled to account for difference in ν_{ave}, $\Delta\nu$, and $\vartheta(T)$. The results in Figure 5 should be multiplied by 1.9 to provide the total k_{rad} of perovskite. I assume that ppv behaves the same.

Maxima exist in k_{rad} as a function of Fe content (Fig. 5, right-hand side). The position of the maxima depends on the grain size, due to the k_{rad} being a function of the product dX (Eq. 21). Because perovskite has a stronger absorption coefficient

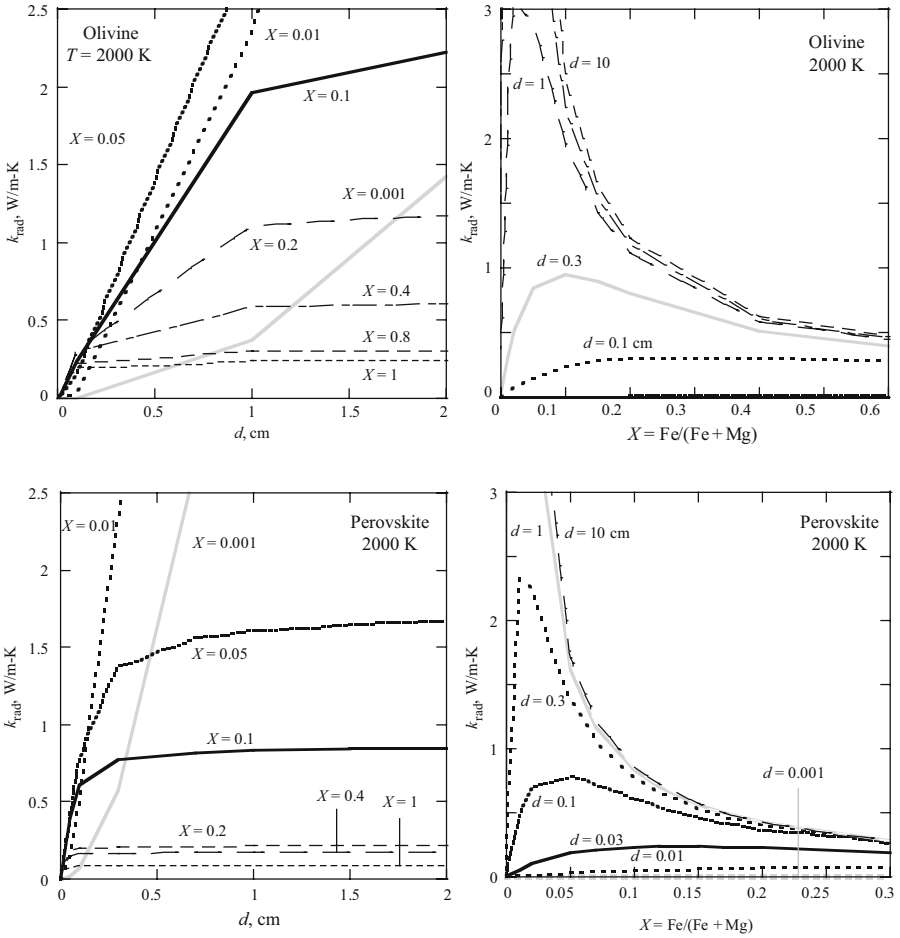


Figure 5. Dependence of $k_{\rm rad}$ (Eq. 21) on d (left panels) and X (right panels). Note difference in axis scales. Curves are labeled with the values of X or d. Upper panels show olivine. Lower panels show perovskite calculated using only the low ν band.

than olivine (i.e., f is larger, Eq. 20), its maxima occur at lower values of X (right panels, Table 3). For most values of d and X, $k_{\rm rad}$ of perovskite is larger than that of olivine, mostly connected to its larger A values. Values of $k_{\rm rad}$ at large dX are overestimated. Accounting for surface reflectivity would sharpen the maxima, but its position should not be affected. At very large dX, the curves would cross, i.e., the $d = 10$ cm curve would approach $k_{\rm rad} = 0$ at smaller X than the $d = 2$ cm curve.

At low concentrations of Fe, $k_{\rm rad}$ increases strongly with grain-size (Fig. 5, left-hand side). For all but the lowest concentrations, a constant value is obtained above about $d = 1$ cm for olivine and above about $d = 0.5$ cm for perovskite. Specifically,

Table 3. Maxima in perovskite k_{rad}

d, cm	X_{max}, Fe/(Mg + Fe)
10	0.001
1	0.01
0.5	0.013
0.1	0.05
0.03	0.12
0.01	0.38

the plateau occurs at d values that inversely correlate with $X = \mathrm{Fe}/(\mathrm{Fe} + \mathrm{Mg})$, i.e., at $X = 0.1$, the plateau is at 0.5 cm whereas at $X = 0.2$, the plateau occurs at $d = 0.2$ cm. The plateau exists because k_{rad} is overestimated at large dX. Instead, a maximum is expected, such that the grain-size where the maximum occurs would decrease as X increases.

3.3.3 Low spin iron

Spectra of silicates with low spin Fe^{2+} are unavailable to the best of our knowledge. However, transformation from the high to low spin state should eliminate the d-d transitions at low ν, but some of the high frequency bands, i.e., transitions to spin-forbidden states, will remain. For perovskite, the band at 15,200 cm^{-1} will disappear if this is a d-d transition, but will remain if it involves Fe^{2+}-Fe^{3+} charge transfer.

If perovskite does indeed have charge transfer, then the low spin state will have $\vartheta(T)$ that is $1/10^{th}$ the value calculated for the d-d transitions of high spin Fe^{2+}. The remaining components of k_{rad} (cf. Eqs. 21 and 22) depend on ν_{ave}, $\Delta\nu$, d and X. Because strengths of the low and high ν bands are essentially the same, the results in Figure 5 for the low ν, d-d bands need only be scaled. From Table 2, the results for high spin perovskite in Figure 5 should be multiplied by 0.9 to depict the low spin state. If charge transfer exists, thermal conductivity is decreased only by a factor of 2 by the spin state transformation, and the shape of the curves, i.e., $k_{rad}(X)$, remains the same.

If the band at 15,200 cm^{-1} is instead the third d-d transition in high spin perovskite, then the low spin state will consist of a UV tail and some weak absorptions in the visible region. Spin forbidden bands are $\sim 1/100^{th}$ the intensity of d-d transitions in the high spin state, and also have much narrow widths which may change f. As a first approximation, widths should be $1/100^{th}$ that of the d-d bands. Frequencies would resemble the high ν band in Table 2. The Y-axis in Figure 5 would therefore be scaled down by a factor of $\sim 1/100^{th}$ to account for the change in s and ϑ. From Equation 20, the X values should be multiplied by a large factor, on the order of 100, to account for lower absorbance. In summary, values of thermal conductivity would be much lower in the high spin state, and the maximum in X is shifted to near the iron end-member, if the high spin spectrum consists only of d-d transitions.

Badro et al. (2004) reached the opposite conclusion that $k_{\rm rad}$ is large for the low spin state of Fe^{2+} owing to its low A values. They neglected to account for the effect of grain-size on radiative transfer (Hofmeister, 2005). To the contrary, the effect of scattering is very strong at low A (Eq. 13) causing $k_{\rm rad}$ to be small for pale materials, including those with low spin Fe^{2+}. This behavior is clear from the asymptotic limit (Eqs. 14 or 16), or by simply considering the size of the mean free path $= d/(1 + dA) \sim d$.

4 DISCUSSION AND CONCLUSIONS

4.1 Summary of lower mantle heat transport properties

Heat transfer in the deepest mantle is connected with mantle convection processes, including the generation and maintenance of plumes. Thermal conductivity (or diffusivity) influences mantle convection models even in the presence of a strongly temperature dependent viscosity (van den Berg et al., 2004; Yanagawa et al., 2005). Providing exact values of k or D for the lower mantle is not currently feasible due to lack of suitable samples, difficult to attain temperatures, and uncertainties in physical properties used to compute k or D. Problems include the chemical composition not being well-constrained because few mantle samples originate near 670 km and nothing has emerged from greater depths (Gasparik, 2000), and because modeling seismic velocity distribution is equivocal due to tradeoffs in T, chemical composition, and phase (Deschampes and Trampart, 2003). Grain-size is crucial, but is also not well-constrained (Ranalli, 2001). Growth is retarded by shear forces arising during flow, which disrupts and deforms the large grains. Yet, grain growth is promoted by high temperatures and slow motions.

Despite the above problems, the phonon contribution is fairly well constrained. Lower mantle conditions are above $T_{\rm C}$, and thus D (or $k_{\rm lat}$) is independent of temperature (Fig. 1), but increases with pressure (Eq. 9; also see Hofmeister, 2007). The large values in Table 1 allow for the high pressure in the deepest mantle. The bulk modulus and thermal Grüneisen parameters of perovskite and ppv are similar, so the pressure effects are similar. Moreover, changes with pressure are relatively unimportant since it is feedback through the temperature equation that strongly influences mantle convection (Dubuffett et al., 2002). However, $k_{\rm lat}$ increasing upon transformation from perovskite to post-perovskite (Table 1) provides positive $\partial k_{\rm lat}/\partial T$, if this transition is spread over sufficient depth that the temperature changes significantly. This exception is important because the positive derivative promotes stability (Dubuffett et al., 2002). Other gradual phase transformations (excepting spin states) and changes in chemical composition could similar provide thermal gradients in the lattice contribution. Although the trends are clear, the absolute value of D is not, due to variation in the dependence of saturated values on lattice constant (Fig. 2).

Diffusion of radiation should largely govern heat transfer in the lower mantle due to its strong dependence on T (Eqs. 13, 21; Fig. 4) which occurs over great depths. Constraining $k_{\rm rad}$ can be difficult owing to its sensitivity to phase, and strong

dependence on chemical composition and grain size (Eq. 13, Fig. 5). Therefore, the mantle is represented by an approximate analytical solution to Equation 13 that is derived in terms of composition and only loosely connected to spectral parameters (Eq. 21). In lieu of spectral data, post-perovskite is assumed to behave the same as perovskite. The absolute values of $k_{\rm rad}$ are uncertain, although the trends are fairly well constrained. Salient features are that $k_{\rm rad}$ depends roughly linearly on T in the lower mantle, and that maxima in $k_{\rm rad}$ occur as a function of $X = {\rm Fe}/({\rm Fe} + {\rm Mg})$ such that the position depends on the grain-size. A broad maximum exists in $k_{\rm rad}$ as a function of d, and its position depends on X. For a maximum to occur at $X = 0.1$, compositions found in the upper mantle, $d \sim 0.3$ mm in the lower mantle (Fig. 5). Similar behavior, but lower values of $k_{\rm rad}$ are expected for the low spin state, such that X of the maximum is shifted towards the Fe end-member. Radiative transfer is weakened by this transition due to the effect of grain-size shortening the mean free path.

4.2 Implications of deepest mantle heat transfer on plumes

As shown by Matyska and Yuen (2005) radiative heat transfer is important in allowing large lower-mantle plumes to develop in the presence of the post-perovskite phase transition. The simple approach taken here considers, as a guideline for plume formation, the overall stability of the core-mantle boundary layer as indicated by the findings of Dubuffett et al. (2002) and the variable nature of thermal conductivity. Plumes are promoted by instabilities: for example, grains with lower thermal conductivity will retain heat and become buoyant. The temperature derivatives play an even more important role, as shown by Yuen and collaborators.

Thermal conductivity due to lattice vibrations in the layer just above the core-mantle boundary appears to be large, due to the combined effects of pressure, large lattice constants, and the transition from pv to ppv, all of which stabilize against convection. However, increasing Fe content decreases $k_{\rm lat}$ (Hofmeister, 2005) and thus decreases stability (promotes convection). This effect is less important, however, than radiative transport which is strongly temperature dependent, positive and thus quite stabilizing. Transition to the low spin state at moderate to high Fe content would increase $k_{\rm rad}$ (if d is unchanged), contributing to stability. However, transition to the low spin state at low Fe content (if d is unchanged) decreases stability because $k_{\rm rad}$ is reduced. Irrespective of the spin state, increasing grain-size increases $k_{\rm rad}$ and contributes to stability, up to a certain d, which depends on X, such that large d and X are destabilizing.

Thus, whether conditions in the core-mantle boundary layer are or are not conducive to plume formation depends on many variables. Plume formation is most likely under destabilizing conditions of large grains (which can actually be small for high Fe^{2+} content, Fig. 5), or very, very small grains, low to moderate Fe contents for low spin iron, or moderate to high contents for high spin iron. Higher degrees of solid solution (e.g., Al or Ca along with Fe in perovskite) would also favor plume formation.

If conditions in the core-mantle boundary layer have evolved to maximize radiative transfer, then provision of additional Fe^{2+} from the core has implications on plume

formation, as discussed by Hofmeister and Yuen, in review) and summarized here. The decrease in k_{rad} at large d, due to finite surface reflectivity and the decrease in k_{rad} as Fe content increases (Fig. 5) suggest that positive feedback exists. Let us assume that the ultralow velocity zone adjacent to the core provides a source of Fe ions. Then, in the boundary layers, flow is slow which allows grain-growth to proceed. The slowest regions within the boundary layers are stagnation points where upwellings (e.g., plumes) would form. Not only does grain growth in the stagnant regions aid incorporation of new, Fe^{2+}-rich material, but moreover, increased grain-size means that very little increase in Fe^{2+} content is needed to reduce radiative transfer and increase buoyancy. Such positive reinforcement suggests that small changes in Fe content or grain size could initiate the process. Whereas grain growth and Fe enrichment work together to initiate the process, it is the connection of reduced viscosity with Fe content which provides the feedback loop which sustains plume development. Feedback can occur regardless of the spin state of Fe ions, but stability of the low-spin state requires higher concentrations and larger grain-sizes to operate.

The above proposal of Hofmeister and Yuen (under review) addresses the seemingly contradictory result of Trampert et al. (2004) which associates high Fe contents with lower mantle underlying the central Pacific, regions thought to be hotter than ambient due to the density being lower. The existence of thermo-chemical plumes (Yuen et al., 1993; Ishii and Tromp, 1999) engendered by iron enrichment further suggests both chemical differentiation of the lower mantle, and a density stratification consistent with layered convection. Evidence for decoupling of the lower and upper mantle systems is summarized by Hamilton (2003), Anderson (2002), and Foulger et al. (2005).

ACKNOWLEDGEMENTS

Support was provided by NSF EAR 0132275 and 0206121.

REFERENCES

Anderson, D.L. (2002) The case for irreversible chemical stratification of the mantle. *Int. Geol. Rev.*, 44, 97–116.

Anderson, O.L., and D.G. Isaak (1995) Elastic constants of mantle minerals at high temperature. In Ahrens, T.J. (ed.) A Handbook of Physical Constants, American Geophysical Union, Washington D.C., pp. 64–96.

Andre, S., and A. Degiovanni (1995) A theoretical study of the transient coupled conduction and radiation heat transfer in glass: Phonic diffusivity measurements by the flash technique. *Int. J. Heat. Transfer.*, 38, 3401–3412.

Bass, J.D. (1995) Elasticity of minerals, melts, and glasses. In Ahrens, T.J. (ed.) A Handbook of Physical Constants, American Geophysical Union, Washington D.C., pp. 45–63.

Blumm, J., J.B. Henderson, O. Nilson, and J. Fricke (1997) Laser Flash measurement of the phononic thermal diffusivity of glasses in the presence of ballistic radiative transfer. *High Temp. High Press.*, 29, 555–560.

Blumm, J., and S. Lemarchand (2002) Influence of test conditions on the accuracy of laser flash measurements. *High Temp. High Press.*, 34, 523–528.

Braeuer, H., L. Dusza, and B. Schulz (1992) New laser flash equipment LFA 427. *Interceram.*, 41, 489–492.

Branlund, J., M.C. Kameyama, D.A. Yuen, and Y. Kaneda (2000) Effects of temperature-dependent thermal diffusivity on shear instability in a viscoelastic zone: Implication for faster ductile faulting and earthquakes in the spinel stability field. *Earth Planet. Sci. Lett.*, 182, 171–185.

Brewster, M.Q. (1992) Thermal Radiative Transfer and Properties, John Wiley and Sons, Inc., New York.

Buettner, R., B. Zimanowski, J. Blumm, and L. Hagermann (1998) Thermal conductivity of a volcanic rock material (olivine-melilitite) in the temperature range between 298 and 1470 K. *J. Volcan. Geothermal. Res.*, 80, 293–302.

Burns, R.G. (1982) Electronic spectra of minerals at high pressures: How the mantle excites electrons. In Schreyer, W. (ed.) High-Pressure Researches in Geoscience, E. Schweizerbartsche Verlag, Stuttgart, pp. 223–246.

Clark, Jr., S.P. (1957) Radiative transfer in the Earth's Mantle. *Trans. Am. Geophys. Union*, 38, 931–938.

Debye, P. (1914) Vortrage über die kinetische Theorie der Materie und der Electriztät. B.G. Teuber, Berlin, pp. 1–196.

Deschamps, F., and J. Trampert (2003) Mantle topography and its relation to temperature and composition. *Phys. Earth Planet. Inter.*, 140, 277–291.

Dubuffet, F., D.A. Yuen, and E.S.G. Rainey (2002) Controlling thermal chaos in the mantle by positive feedback from radiative thermal conductivity. *Nonlinear Proc. Geophys.*, 9, 1–13.

Dugdale, J.S., and D.K.C. MacDonald (1955) Lattice thermal conductivity. *Phys. Rev.*, 98, 1751–1752.

Dziewonski, A.M., and D.L. Anderson (1981) Preliminary reference Earth model. *Phys. Earth Planet. Int.*, 25, 297–356.

Evans, A. (1992) The Dusty Universe, Ellis Horwood, New York, pp. 1–236.

Foulger, G.R., J.H. Natland, D.C. Presnall, and D.L. Anderson (2005) Melting Anomolies: Their Nature and Origin, Geological Society of America, Boulder Colorado, USA, pp. 1–881.

Fujisawa, H., N. Fujii, H. Mizutani, H. Kanamori, and S. Akimoto (1968) Thermal diffusivity of Mg_2SiO_4, Fe_2SiO_4, and NaCl at high pressures and temperatures. *J. Geophys. Res.*, 75, 4727–4733.

Gasparik, T. (2000) Evidence for the transition zone origin of some [Mg,Fe]O inclusions in diamonds. *Earth Planet. Sci. Lett.*, 183, 1–5.

Geisting, P.A., A.M. Hofmeister, B. Wopenka, G.D. Gwanmesia, and B.L. Jolliff (2004) Thermal conductivity and thermodynamic properites of majorite: Implications for the transition zone. *Earth Planet. Sci. Lett.*, 218, 45–56.

Gerbault, M. (2000) At what stress level is the central Indian Ocean lithosphere buckling? *Earth Planet. Sci. Lett.*, 178, 165–181.

Giesting, P.A., and A.M. Hofmeister (2002) Thermal conductivity of disordered garnets from infrared spectroscopy. *Phys. Rev.*, B65, website paper # 144305 (15 pages).

Hamilton, W.B. (2003) An alternative Earth. *GSA Today*, 13, 2–4.

Hapke, B. (1993) Theory of Reflectance and Emittance Spectroscopy, Cambridge University Press, Cambridge, pp. 1–455.

Henderson, J.B., F. Giblin, J. Blumm, and L. Hagemann (1998) SRM 1460 series as a thermal diffusivity standard for laser flash instruments. *Int. Jour. Thermophysics*, 19, 1647–1656.

Hofer, M., and F.R. Schilling (2002) Heat transfer in quartz, orthoclase, and sanidine at elevated temperature. *Phys. Chem. Mineral.*, 29, 571–584.

Hofmann, R., O. Hahn, F. Raether, H. Mehling, and J. Fricke (1997) Determination of thermal diffusivity in diathermic materials by the laser-flash technique. *High Temp. High Press.*, 29, 703–710.

Hofmeister, A.M. (1999) Mantle Values of Thermal Conductivity and the Geotherm from Phonon Lifetimes. *Science*, 283, 1699–1706.

Hofmeister, A.M. (2001) Thermal conductivity of spinels and olivines from vibrational spectroscopy at ambient conditions. *Am. Mineral.*, 86, 1188–1208.

Hofmeister, A.M. (2004a) Enhancement of radiative transfer in the mantle by OH- in minerals. *Phys. Earth Planet. Inter.*, 146, 483–485.

Hofmeister, A.M. (2004b) Thermal conductivity and thermodynamic properties from infrared spectroscopy. In King, P., M. Ramsey, and G. Swayze (eds.) Infrared Spectroscopy in Geochemistry, Exploration Geochemistry, and Remote Sensing, Mineralogical Association of Canada, Ottawa, Ontario, pp. 135–154.

Hofmeister, A.M. (2004c) Physical properties of calcium aluminates from vibrational spectroscopy. *Geochim. Cosmochim. Acta.*, 68, 4721–4726.

Hofmeister, A.M. (2005) The dependence of radiative transfer on grain-size, temperature, and pressure: Implications for mantle processes. *J. Geodynamics*, 40, 51–72.

Hofmeister, A.M. (2006) Thermal diffusivity of garnets at high temperature. *Phys. Chem. Mineral.* 33, 45–62.

Hofmeister, A.M. (2007) Pressure dependence of thermal transport properties. Proceedings of the National Academy of Science, doi: 10.1073/pnas.0610734104.

Iitaka, T., K. Hirose, K. Kawamura, and M. Murakami (2004) The elasticity of the MgSiO3 post-perovskite phase in the Earth's lowermost mantle. *Nature*, 430, 442–445.

Ishii, M., and J. Tromp (1999) Normal-mode and free-air gravity constraints in lateral variations of velocity and density in Earth's mantle. *Science*, 285, 1231–1236.

Julian, C.L. (1965) Theory of heat conduction in rare-gas crystals. *Phys. Rev.*, A137, 128–137.

Kachare, A., G. Andermann, and L.R. Brantley (1972) Reliability of classical dispersion analysis of LiF and MgO reflectance data. *J. Phys. Chem. Solids*, 33, 467–475.

Kanamori, H., N. Fujii, and H. Mizutani (1968) Thermal diffusivity measurement of rock-forming minerals from 300 to 1100 K. *J. Geophys. Res.*, 73, 595–603.

Kaufmann, R., and W.J. Freedman (2002) Universe, W.H. Freeman, New York.

Keppler, H., C.A. McCammon, and D.C. Rubie (1994) Crystal-field and charge-transfer spectra of $(Mg,Fe)SiO_3$ perovskite. *Am. Mineral.*, 79, 1215–1218.

Keppler, H., and C.A. McCammon (1996) Crystal-field and charge-transfer spectra of $(Mg,Fe)SiO_3$ majorite. *Phys. Chem. Mineral.*, 23, 94–98.

Khomenko, V.M., K. Langer, R. Wirth, and B. Weyer (2001) Mie scattering and charge transfer phenomena as causes of the UV edge in the absorption spectra of natural and synthetic almandine garnets. *Phys. Chem. Mineral.*, 29, 201–209.

Klemens, P.G. (1969) Theory of the thermal conductivity of solids. In Tye, R.P. (ed.) Thermal Conductivity, Academic Press, New York, pp. 1–68.

Lee, D.W., and W.D. Kingery (1960) Radiation energy transfer and thermal conductivity of ceramic oxides. *J. Am. Ceram. Soc.*, 43, 594–607.

Liebfried, G., and E. Schlömann (1954) Warmleitund in elektrische isolierenden Kristallen. *Nach Ges Wissenschaften Goettingen Mathematik und Physik* K1, 71–93.

Mao, W., G. Shen, V.B. Prakapenka, Y. Meng, A.J. Campbell, D.L. Heinz, J. Shu, R.J. Hemley, and H.K. Mao (2004) Ferromagnesian postperovskite silicates in the D″ layer. *Proc. Natl. Acad. Sci.*, 39, 15867–15869.

Matyska, C., and D.A. Yuen (2005) The importance of radiative heat transfer on superplumes in the lower mantle with the new post-perovskite phase change. *Earth Planet Sci. Lett.*, 234, 71–81.

McCammon, C.A., D.C. Rubie, C.R. Ross II, F. Siefert, and HStC O'Neill (1992) Mössbauer study of $^{57}Fe_{0.05}Mg_{0.95}SiO_3$ perovskite at 80 and 298 K. *Am. Mineral.*, 77, 894–897.

Mehling, H., G. Huatzinger, O. Nilsson, J. Fricke, R. Hofmann, and O. Hahn (1998) Thermal diffusivity of semitransparent materials determined by the laser-flash method: Applying a new analytical model. *Int. J. Thermophys.*, 19, 941–949.

Mitra, S.S. (1969) Infrared and Raman spectra due to lattice vibrations. In Nudelman, S., and S.S. Mitra (eds.) Optical Properties of Solids, Plenum Press, New York, pp. 333–452.

Murakami, M., K. Hirose, K. Kawamura, N. Sata, and Y. Ohishi (2004) Post-perovskite phase transition in $MgSiO_3$. *Science*, 30, 855–858.

Oganov, A.R., and S. Ono (2004) Theoretical and experimental evidence for a post-perovskite phase of $MgSiO_3$ in Earth's D″ layer. *Nature*, 430, 445–448.

Parker, J.W., J.R. Jenkins, P.C. Butler, and G.I. Abbott (1961) Flash method of determining thermal diffusivity, heat capacity, and thermal conductivity. *J. Appl. Phys.*, 32, 1679–1684.

Peierls, R.E. (1929) Zur kinetische Theorie der Warmeleitung in Kristallen. *Ann der Physik Leipzig*, 3, 1055–1101.

Peierls, R.E. (1956) Quantum Theory of Solids, Clarendon Press, Oxford, 229pp.

Pertermann, M., and A.M. Hofmeister (2006) Thermal diffusivity of olivine-group minerals. *Am. Mineral.*, 91, pp. 1747–1760.

Pomeranchuk, I. (1943) Heat conductivity of dielectrics at high temperatures. *J. Phys. USSR*, 7, 197–201.

Ranalli, G. (2001) Mantle rheology: Radial and lateral viscosity variations inferred from microphysical creep laws. *J. Geodynam.*, 32, 425–444.

Reif, F. (1965) Fundamentals of Statistical and Thermal Physics, McGraw Hill Book Co., New York, pp. 1–651.

Ross, R.G., P. Andersson, B. Sundqvist, and G. Bäckström (1984) Thermal conductivity of solids and liquids under pressure. *Rep. Prog. Phys.*, 47, 1347–1402.

Rossman, G.R. (1988a) Optical spectroscopy. *Rev. Mineral.*, 18, 207–254.

Rossman, G.R. (1988b) Vibrational spectroscopy of hydrous components. *Rev. Mineral.*, 18, 193–206.

Roufosse, M.C., and P.G. Klemens (1973) Thermal conductivity of complex dielectric crystals. *Phys. Rev.*, B7, 5379–5386.

Roufosse, M.C., and P.G. Klemens (1974) Lattice thermal conductivity of minerals at high temperatures. *J. Geophys. Res.*, 79, 703–705.

Schilling, F.R. (1999) A transient technique to measure thermal diffusivity at elevated temperatures. *Eur. J. Mineral.*, 11, 1115–1124.

Shankland, T.J., U. Nitsan, and A.G. Duba (1979) Optical absorption and radiative heat transport in olivine at high temperature. *J. Geophys. Res.*, 84, 1603–1610.

Smyth, J., and T. McCormick (1995) Crystallographic data for minerals. In Ahrens, T.J. (ed.) A Handbook of Physical Constants, American Geophysical Union, Washington D.C., pp. 1–17.

Spitzer, W.G., R.C. Miller, D.A. Kleinman, and L.W. Howarth (1962) Far–infrared dielectric dispersion in $BaTiO_3$, $SrTiO_3$, and TiO_2. *Phys. Rev.*, 126, 1710–1721.

Tan, H.P., B. Maestre, and M. Lallemand (1991) Transient and steady-state combined heat transfer in semitransparent materials subjected to a pulse or step irradiation. *J. Heat. Transfer*, 113, 166–173.

Taran, M.N., and K. Langer (2001) Electronic absorption spectra of Fe^{2+} ions in oxygen-based rock-forming minerals at temperatures between 297 and 600 K. *Phys. Chem. Minerals*, 28, 199–210.

Trampert, J., F. Deschamps, J. Resovsky, and D.A. Yuen (2004) Probabilistic tomography maps chemical heterogeneities in the lower mantle. *Science*, 306, 853–856.

Tsuchiya, T., J. Tsuchiya, K. Umemoto, and R.M. Wentzcovitch (2004) Phase transition in $MgSiO_3$ perovskite in the earth's lower mantle. *Earth Planet. Sci. Lett.*, 224, 241–248.

Van den Berg, A.P., D.A. Yuen, and E.S.G. Rainey (2004) The influence of variable viscosity on delayed cooling due to variable thermal conductivity. *Phys. Earth Planet Inter.*, 142, 283–295.

Yanagawa, T.K.B., M. Nakada, and D.A. Yuen (2005) The influence of lattice thermal conductivity on thermal convection with strongly temperature-dependent viscosity. *Earth Space. Sci.*, 57, 15.

Yuen, D.A., A.P. Vincent, S.Y. Bergeron, F. Dubuffet, A.A. Ten, V.C. Steinbach, and L. Starin (2000) Crossing of scales and nonlinearities in geophysical processes. In Boschi, E., G. Ekstrom, and A. Morelli (eds.) Problems in Geophysics for the New Millenium, Editrice Compositori, Bologna, Italy, pp. 405–465.

Ziman, J.M. (1962) Electrons and Phonons: The Theory of Transport Phenomena in Solids, Clarendon Press, Oxford (Ch 8 and 11), pp. 1–554.